IEEE Photonics Journal
An IEEE Photonics Society Publication

Open Access

Modification of Level Dependent ASE-Signal Beat Noise by Optical and Electrical Filtering in Optically Preamplified Direct Detection Receivers

Volume 10, Number 1, February 2018

J. Witzens
J. Müller
A. Moscoso-Mártir

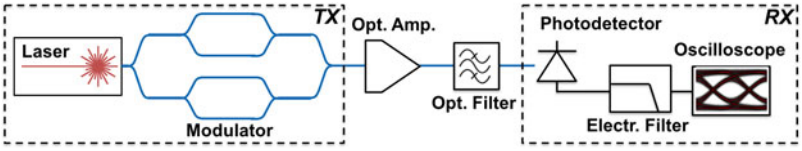

DOI: 10.1109/JPHOT.2017.2785287
1943-0655

IEEE photonics SOCIETY

IEEE

Modification of Level Dependent ASE-Signal Beat Noise by Optical and Electrical Filtering in Optically Preamplified Direct Detection Receivers

J. Witzens, J. Müller, and A. Moscoso-Mártir

Institute of Integrated Photonics, RWTH Aachen University, Aachen 52074, Germany

DOI:10.1109/JPHOT.2017.2785287

Manuscript received November 7, 2017; revised December 12, 2017; accepted December 13, 2017. Date of publication December 19, 2017; date of current version January 23, 2017. This paper has supplementary downloadable material available at http://ieeexplore.ieee.org. Corresponding author: J. Witzens (e-mail: jwitzens@iph.rwth-aachen.de).

Abstract: We derive compact equations describing the modification of amplified spontaneous emission signal beat noise arising from optical and electrical filtering in optically preamplified direct detection receivers. In particular, we show that this modification typically results in a further decrease of the signal quality factor. This is particularly pronounced in the presence of electrical filters with steep transfer functions such as, e.g., occurring when feeding the signal through an antialiasing filter prior to analog-to-digital conversion or in a real-time oscilloscope, in the latter case leading to counter-intuitive dependencies of the measured signal quality on the characteristics of the test setup. Predictions are exemplified in concrete system models and verified with experiments. While the modeling assumptions and the accuracy of the predictions are in line with models previously reported in the literature, derived expressions allow straightforwardly tying the modification of the level dependent noise to signal levels, baud rate, signal spectrum, and filter transfer functions.

Index Terms: Laser amplifiers, electro-optical systems, optical interconnects, amplified spontaneous emission, direct detection opto-electronic receivers.

1. Introduction

With the advent of the first commercial erbium doped fiber amplifiers (EDFAs) in the late eighties, amplified spontaneous emission (ASE) noise has become an essential aspect of optical communications and is now a well-understood phenomenon that has been intensely investigated. Comprehensive models for example take into account deviations from non-Gaussian noise statistics in direct detection systems [1]–[3]. While they have been shown to result in very similar signal qualities as predicted by simpler Gaussian noise models [3], the predicted optimum decision thresholds are significantly different. Another difficulty associated to the modeling of optically preamplified direct detection receivers (Rx) resides in the modeling of level dependent noise in the presence of arbitrary optical and electrical filtering [4]–[13]. Comprehensive models have been derived for optically preamplified Rx based on the Gaussian noise approximation [4]–[7] and have been shown to predict signal qualities in close agreement with experimental results when level dependent ASE-signal beat noise is properly modeled [8]. More advanced statistical models take into account the chi square distribution of ASE noise in optically and electrically filtered optically preamplified Rx [9]–[13].

Here, we make the same approximations in the modeling of ASE noise as in [4]–[7], in that ASE-signal beat noise is modeled independently of ASE-ASE beat noise. The resulting Gaussian ASE-signal beat noise variance can then be further utilized in the framework of the Gaussian noise approximation in order to obtain a comprehensive link model. The objective is not to increase the accuracy compared to previous works reported in [4]–[7], as a matter of fact numerically evaluated ASE-signal beat noise would be exactly the same since the underlying set of assumptions is identical, but rather to obtain a compact set of equations that straightforwardly reveal the dependence of filtered, level dependent ASE-signal beat noise on signal levels (in particular signal extinction ratio), signal power spectral density (PSD), optical filter cutoff-frequency, electrical filter cutoff frequency and electrical filter shape, as well as pattern dependencies. In [4]–[7] the analysis is based on the optical and electrical filters' impulse responses as well as on a real-time description of the signal's optical field amplitude. Here, on the other hand, results are expressed in terms of Fourier domain characteristics, which makes the aforementioned trends readily apparent, providing further guidance for system design or for the interpretation of system characterization data. As in previous works, use of the Gaussian approximation is justified by the fact that resulting errors in the estimated Bit Error Ratio (BER) remain small for direct detection amplitude modulated systems. It is a well-known limitation of the Gaussian approximation that it is only accurate if the ratio M of the optical filter bandwidth with the electrical filter bandwidth is significantly larger than one [1], [2], [14]. When the optical filter bandwidth is comparable to the electrical filter bandwidth, resulting discrepancies lead to errors in the predicted BER that are particularly pronounced in the case of differential phase shift keying (DPSK). In the case of direct detection on-off keying (OOK) on the other hand, while the Gaussian approximation leads to significant errors in the predicted optimal threshold level, the predicted BER is usually quite accurate, even at low M (see for example [2, Fig. 5] for a comparison of predicted BER accuracy for DPSK and OOK as a function of M). Nonetheless, care should be taken to verify the domain of validity of the Gaussian approximation when working on a specific system architecture. It is further verified here based on numerical investigation of a model system in which the optical and electrical filter bandwidths are equal to each other and both set to twice the signal's Nyquist frequency that the corrections introduced by a complete treatment of ASE-signal beat noise can be of a significantly higher magnitude than the errors introduced by the Gaussian noise approximation, i.e., this approach can significantly improve the predictive quality of modeling results while remaining in the framework of the Gaussian approximation.

In the following, the modification of the ASE-signal beat noise is parameterized by two numbers, denoted as μ and γ, that are a function of the electrical and optical filter shapes as well as the symbol shape at the input of the receiver. While these coefficients are, in the general case, pattern dependent, i.e., their exact value depends on the sequence of symbols in which the analyzed symbol is embedded, once calculated they allow for example to straightforwardly assess modified ASE-signal beat noise at different signal extinction ratios and provide intuition on how the ASE-signal beat noise modification varies with signal rate. Moreover, with an additional assumption (independent, linearly superimposed symbols in a linear optical channel), general pattern independent expressions for average noise variances are given that can be straightforwardly evaluated for each symbol category and are compatible with the modeling of multi-level signaling.

Few limiting assumptions enter the derivations of the general case: Optical and electrical filters are arbitrary linear filters, the latter also including channel equalization filters. Moreover, the signal optical field amplitude entering the Rx can be arbitrarily shaped and complex valued. The spectrum of the optical noise can also be arbitrarily shaped by the choice of optical filter, since optical noise is assumed to be filtered white noise, while the assumed signal shape is independently described post optical filtering at the entrance to the Rx right before detection. Dispersion occurring prior to the optical amplifier or between the latter and the photodetector is fully accounted for.

A limitation, however, lies in the assumption of the optical noise to be fully uncorrelated from the data stream, as is for example the case at the output of an ideal optical amplifier followed by a linear fiber link. Correlations occurring for example due to relative intensity noise, post amplification modulation, or due to a signal level dependent noise figure in a saturating semiconductor optical amplifier (SOA), are not rigorously modeled here. While amplification by an EDFA is adequately

modeled as its noise figure does not vary at the time scale of the data, correlations induced between the signal and the optical noise due to fiber nonlinearities after amplification are not taken into account in the modeling framework presented here. The latter is however a subtle effect, so that the formulas remain widely applicable.

As already mentioned, a second set of equations is given for a slightly less general case, in which it is assumed that the data stream is composed of a linear superposition of symbols. This second framework still handles dispersion (and the interference of overlapping symbols), but does not allow a rigorous modeling of fiber and amplifier nonlinearities (e.g., self- and cross gain modulation in an SOA). It does, however, have the advantage that average values of μ and γ can be straightforwardly calculated for each symbol category, allowing for example the quick assessment of measurement bias when characterizing with a real-time oscilloscope.

While the modification of the level-dependent ASE-signal beat noise as compared to simple models based on instantaneous signal levels and filter noise equivalent bandwidths (NEBs) appears to be relatively weak in many practical system configurations, its inclusion in system models has already been shown to yield significant improvements of modeling accuracy in practical cases, as evidenced by comparison with experiments [8]. It is particularly pronounced in systems whose post-detection filtering is limited by electrical filters with a sharp roll-off. This is for example the case when an optical signal quality is monitored with a real-time oscilloscope, since the latter typically filters the signal with what is intended to be as close as possible to an ideal square shaped filter. In such a setting, typical test system specific penalties exceeding 0.5 dBQ have been recorded and adequately modeled (with dBQ defied as $20\log_{10}(Q_{sig})$ and Q_{sig} the signal quality factor). Moreover, feeding a signal through a square shaped anti-aliasing filter in a receiver prior to analog-to-digital conversion, e.g., in a direct detection digital multitone (DMT) Rx, equally impacts the signal-ASE beat noise.

The reported formulas allow calculating the ASE-signal beat noise variance for a large class of amplified, direct detection optical systems. While direct detection systems are legacy systems in long haul communications and might be progressively phased out, amplification might become increasingly important in high baud rate short range communications: As serial data rates rise, link budgets might become increasingly difficult to meet without amplification even at very short distances. As an example, in [15] authors showed 64 Gb/s OOK transmission over 2 km by means of a distributed feedback laser (DFB) combined with an electro-absorption modulator (EAM) at the transmitter and an SOA pre-amplified receiver. A silicon photonics dense wavelength division multiplexed (WDM) architecture has been described in [16], [17], in which amplification after modulation serves to compensate the relatively high laser-to-chip and chip-to-fiber insertion losses associated with the technology, as well as modulation penalty arising from limited chip-scale driving voltages. As Baud rates increase to above 50 Gbaud and 4-level pulse amplitude modulation (PAM4) is introduced into 400 G Ethernet modules, post-modulation amplification might also find its way into silicon photonics parallel single mode (PSM) solutions, even though it is still currently considered to be undesirable due to increased packaging complexity and increased power consumption. In particular, optical link budgets based on available DFB lasers do not scale favorably beyond 100 Gbps/lane due to high interface losses and high free-carrier induced losses in modulators, so that less conventional improvement paths such as improved hybrid modulators [18]–[22] and post-modulation amplification [16], [17] might become of higher industrial relevance in the future.

Nonlinearities occurring in the fiber or in an SOA driven into saturation can play an important role in some systems. Such a system configuration can e.g., be found in [23] in which the SOA was purposefully driven into saturation in order to generate a chirp with the opposite sign as the one arising in the EAM, so as to achieve chirp cancellation. Another reason for which an SOA may be driven into partial saturation is to maximize power efficiency in a WDM system [17]. In these instances, the most general formulas derived below remain applicable in that they allow for an arbitrary signal waveform at the input of the Rx (assuming correlation between signal and optical noise due to e.g., a varying noise figure is ignored), while the more restrictive assumption of independent, linearly superimposed symbols is obviously broken, so that the second set of formulas predicting level dependent noise modification as averaged for a given symbol over all patterns becomes approximate.

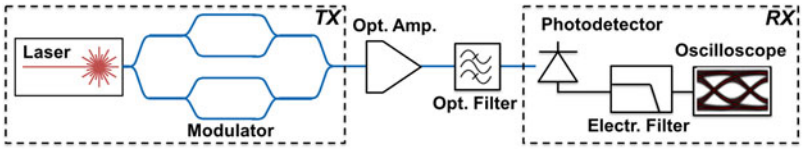

Fig. 1. Diagram of the modeled system: A modulated signal is optically amplified, fed through an optical filter, transduced, low pass filtered and analyzed for signal quality.

The next section is dedicated to a description of the most important analytical formulas, whose complete derivation can be found in the Supplementary Materials. We first describe the simple case corresponding to a sinusoidal signal. It is quite instructive, as these results already contain most of the significant trends, give an order of magnitude of the introduced correction compared to simpler models, and are much easier to derive (Appendix I in the Supplementary Materials). In particular, this simple scenario already shows that the net effect of the ASE-signal beat noise modification is a worsening of the 0-level noise, an improvement of the 1-level noise, and, importantly, typically a net reduction of the signal quality (Q-)factor. Moreover, it is representative for rapidly changing '..01010..' data sequences. Next, we generalize the formula to an arbitrary complex valued signal (derivations in Appendix II). In addition to predicting data sequence dependent noise modifications in the general case, changes to the averaged level dependent noise variances are also predicted for each symbol of a multi-level non-return-to-zero (NRZ) signal in view of facilitating interpretation of Q-factor measurements (derivations in Appendix III). Dependencies on signal and filter characteristics are discussed.

Section 3 describes an experimental validation of the predicted modification of averaged 0- and 1-level noise variances in the case of an OOK NRZ signal. Section 4 continues with a number of numerical signal flow simulations that are used to further exemplify the magnitude of the correction under different system assumptions, as well as to further exemplify pattern dependent effects. Section 5 compares predictions including ASE-ASE beat noise in the framework of the Gaussian noise approximation to more rigorous results stemming from a complete numerical noise modeling taking the non-Gaussian nature of ASE noise in direct detection systems into account.

2. Theoretical Results

Fig. 1 depicts the diagram of the analyzed system. Continuous wave (CW) light is first modulated prior to being optically amplified, optically filtered, transduced into the electric domain and finally electrically filtered. The modulator is represented as an IQ modulator to exemplify the fact that the derived model is compatible with arbitrary complex modulation, for example single sideband modulation in a direct detection system. The optical amplifier is assumed to generate ASE with a white noise PSD that is fully uncorrelated from the data, as is for example the case for an ideal EDFA or an SOA operated in the linear regime. The photodetector is modeled as an ideal element with an output current proportional to the field amplitude squared. The optical and electrical filters are assumed to be linear with no further restrictions. In particular, the case of channel equalization is covered by a general expression of the electrical filter transfer function. In this configuration, there are no restrictions on fiber dispersion, however the fiber is tacitly assumed to be linear to maintain the assumption of uncorrelated ASE up to the input of the receiver. The data stream's signal amplitude is described at the input of the Rx, so that the optical filter transfer function plugged into the formulas can in principle be independently chosen to result in a targeted ASE spectrum at the input of the Rx. The electrical filter can be followed by either a limiting amplifier or faster sampling by an analog-to-digital converter (ADC): In the latter case the general formulas reported below still hold and merely need to be evaluated at the additional relevant sampling times.

We start by reporting formulas derived in the much-simplified case of a signal with a sinusoidal optical field magnitude. These formulas are not only much simpler to derive than the more general

cases of arbitrary signals and random data streams, they also provide an interpretation of the more general formulas, feature the same trends and provide an order of magnitude of the introduced correction (see Appendix I in the Supplementary Materials for their complete derivation).

The characteristics of the optical link are described as follows: G is the optical power gain between the input of the optical amplifier and the input of the Rx, right before the photodetector, and F is the associated noise factor. In other words, both numbers also take into account optical losses occurring between the optical amplifier and the Rx, such as insertion losses of the optical filter. These numbers only enter the expression of the ASE power spectral density (see N_n as defined below), so that the assumption of linearity is not binding (the restrictive assumption is the independence of the generated ASE from the data stream). The optical filter has an optical field baseband transfer function denoted as $\mathcal{F}_o(f)$ in the general case, wherein f is the offset frequency between a signal or noise component and the optical carrier frequency. In the special case where the optical filter is assumed to be an idealized square shaped filter and the optical carrier frequency is assumed to be centered relative the optical filter passband, the width of the optical passband is denoted as $2f_{OF}$, in which case f_{OF} can be seen to be the equivalent single sided cutoff frequency of the filter. Similarly, the electrical filter has a voltage transfer function $\mathcal{F}_e(f)$ in the general case, wherein f is the signal frequency. In the special case where the electrical filter has an idealized square transfer function, its cutoff frequency is denoted as f_{EF}. Without loss of generality, the electrical filter transfer function is assumed not to introduce a time delay (τ_d). In the general case where it does, $\mathcal{F}_e(f)$ should simply be replaced by $\mathcal{F}_e(f_n)e^{i2\pi f\tau_d}$ in the equations, i.e., with the time delay normalized out.

To simplify notations, we introduce $N_n = GFh\nu_0/2$, where h is Planck's constant and ν_0 is the optical carrier frequency (N_n is the PSD of the ASE generated with the same polarization as the signal). We also introduce the NEB of the cascaded optical and electrical filters given by

$$f_F = \frac{1}{2}\int_{-\infty}^{\infty} |\mathcal{F}_e(f_n)|^2 |\mathcal{F}_o(f_n)|^2 df_n \tag{1}$$

where the integral is taken over both positive and negative frequencies to account for situations where the carrier frequency is not centered relative to the optical filter passband or where the optical filter passband is asymmetric. With these definitions, the standard deviation (std. dev.) of the ASE-signal beat noise at constant signal levels, expressed as an input referred optical amplitude, would be simply given by

$$\bar{\sigma} = \sqrt{4N_n \cdot |A_{Rx}|^2 f_F} \tag{2}$$

where A_{Rx} is the optical field amplitude at the input of the Rx normalized as the square root of power. We introduce the two additional frequencies (and a linear combination thereof) defined as

$$\begin{aligned}
f_A &= \frac{1}{2}\int_{-\infty}^{\infty} Re\left(\mathcal{F}_e(f_n)\left[2\mathcal{F}_e(f_n) - \mathcal{F}_e(f_n+f_N) - \mathcal{F}_e(f_n-f_N)\right]^*\right)|\mathcal{F}_o(f_n)|^2 df_n \\
f_B &= \frac{1}{4}\int_{-\infty}^{\infty} |2\mathcal{F}_e(f_n) - \mathcal{F}_e(f_n+f_N) - \mathcal{F}_e(f_n-f_N)|^2 |\mathcal{F}_o(f_n)|^2 df_n \\
f_C &= 2f_A - f_B = \frac{1}{2}\int_{-\infty}^{\infty} \begin{pmatrix} 2|\mathcal{F}_e(f_n)|^2 - Re\left(\mathcal{F}_e(f_n+f_N)\,\mathcal{F}_e(f_n-f_N)^*\right) \\ -|\mathcal{F}_e(f_n+f_N)|^2/2 - |\mathcal{F}_e(f_n-f_N)|^2/2 \end{pmatrix} |\mathcal{F}_o(f_n)|^2 df_n
\end{aligned} \tag{3}$$

With these definitions, a compact form of the modified (post electrical filtering, but input referred) 0- and 1-level signal-ASE beat noise std. dev. is given by

$$\begin{aligned}
\sigma_{0/1} &= \sqrt{4N_n \cdot \left[A_{Rx,0/1}^2 f_F \pm \frac{1}{2}A_{Rx,0/1}\left(A_{Rx,1} - A_{Rx,0}\right) f_A + \frac{1}{8}(A_{Rx,1} - A_{Rx,0})^2 f_B\right]} \\
&= \sqrt{4N_n \cdot \left[A_{Rx,0/1}^2 f_F \pm \frac{1}{4}\left(A_{Rx,1}^2 - A_{Rx,0}^2\right) f_A - \frac{1}{8}(A_{Rx,1} - A_{Rx,0})^2 f_C\right]}
\end{aligned} \tag{4}$$

wherein it should be noted that here A_{Rx} is assumed to be real valued (as opposed to the general case of an arbitrary complex valued signal described in the following).

f_A, f_B and f_C only depend on the oscillation frequency f_N of the sinusoidal optical field amplitude of the signal, i.e., its Nyquist frequency if it is taken to represent a '0101' data stream, as well as on the optical and electrical filter transfer functions. It is already apparent that they are quite sensitive to the steepness of the electrical filter transfer function, via the terms $2\mathcal{F}_e(f_n) - \mathcal{F}_e(f_n + f_N) - \mathcal{F}_e(f_n - f_N)$. The required steepness for (4) to result in a sizeable correction can be further quantified: The electrical filter transfer function needs to significantly change over a frequency span of $2f_N$ in a frequency range in which the ASE is furthermore not filtered out by the optical filter.

As f_A and f_C are typically positive numbers on the order of f_N for typical system configurations (see (A1.8) in Appendix I), (4) can be seen to result in an increase of the 0-level noise std. dev. σ_0 and a decrease of the 1-level noise σ_1. As discussed in Appendix I, the sum of the modified 0- and 1-level std. dev. $\sigma_0 + \sigma_1$ is generally larger than the equivalent quantity for static signal levels calculated according to (2), $\bar{\sigma}_0 + \bar{\sigma}_1$, leading to a decrease of the signal Q-factor once this modification is taken into account. A numerical analysis of (4) shows that the modification $(\sigma_0 + \sigma_1) - (\bar{\sigma}_0 + \bar{\sigma}_1)$ is particularly pronounced at high signal extinction ratios.

If rectangular optical and electrical filter shapes are assumed, and the optical carrier is further assumed to be centered relative to the optical filter bandwidth, these expressions can be further simplified. While in the most general case these assumptions are of limited practical use since, as already mentioned, the effect depends highly on the electrical filter edge steepness, they provide a further guide to intuition (with an explicit dependence of the modified ASE-signal beat noise on data rate), as well as an upper bound of the modification. Moreover, assuming a square shaped optical filter transfer function does not fundamentally modify the results (the expressions of f_A, f_B and f_C given in (3) are not very sensitive to the exact optical filter shape), whereas a square shaped electrical filter does correspond to some practical situations (e.g., real-time oscilloscope or anti-aliasing filter before an ADC). We then obtain $f_F = \min(f_{EF}, f_{OF})$. Further assuming $f_{EF} \geq f_N$ and $f_{OF} \geq f_{EF} + f_N$ (the formulas for all the other cases are given in Appendix I, (A1.8)), we get $f_A = f_C = f_N$ and thus

$$\sigma_{0/1} = \sqrt{4N_n \cdot \left[A^2_{Rx,0/1} f_{EF} \pm \frac{1}{4}\left(A^2_{Rx,1} - A^2_{Rx,0}\right) f_N - \frac{1}{8}(A_{Rx,1} - A_{Rx,0})^2 f_N\right]} \tag{5}$$

i.e., the modification is all the more pronounced the higher the signal frequency relative to the filters' NEB $f_F = \min(f_{EF}, f_{OF})$ and thus the higher the data rate.

Another interesting trend consists in a reduction of f_A and f_B as the optical cutoff frequency f_{OF} is reduced below $f_{EF} + f_N$ (see (A1.8a)). In particular, when $f_{EF} \geq f_{OF} + f_N$, both f_A and f_B are equal to zero and the ASE-signal beat noise can be taken to simply depend on the instantaneous signal levels (in the general case this situation is generalized to $f_{EF} \geq f_{OF} + f_{\max}$, wherin $f_{\max}$ is the maximum signal frequency in the optical amplitude domain).

We can already see that the modification is sufficiently pronounced to be of practical relevance in the case of a square electrical filter: If we assume $f_{OF} \geq f_{EF} + f_N$, infinite extinction ratio, as well as the electrical filter cutoff frequency to be equal to the Nyquist frequency, the expressions further simplify into $\bar{\sigma}_0 + \bar{\sigma}_1 = \sqrt{4N_n A^2_{Rx,1} f_{EF}}$ and $\sigma_0 + \sigma_1 = \sqrt{\frac{1}{8} 4N_n A^2_{Rx,1} f_{EF}} + \sqrt{\frac{5}{8} 4N_n A^2_{Rx,1} f_{EF}}$, which corresponds to a penalty of 1.17 dBQ. While in a realistic system the penalty will be typically reduced both due to the filter and signal shapes (in particular optical filtering, finite electrical filter edge steepness, finite extinction ratio and dominance of other sources of noise each reduce the penalty), this number already provides a rough order of magnitude and a typical upper bound.

Similar formulas are derived for the general case of a random, arbitrarily shaped complex valued data stream in Appendix II. Equation (4) is generalized with the expressions for f_A and f_C replaced by more general quantities denoted as μf_N and γf_N in the following (since the magnitudes of f_A and f_C are generally on the order of f_N, μ and γ are on the order of 1). In the general case, μ and γ are pattern specific, so that they have to be reevaluated for every symbol or sample of a sequence to accurately predict the BER. Averaged quantities are however also reported in the following. These

are particularly useful to evaluate the experimental bias introduced by equipment during signal characterization such as Q-factor measurements.

The field amplitude at the input of the Rx is expressed as a sum of its Fourier components as

$$A_{Rx}\ (t) = \frac{a}{2}\ + \int_{-\infty}^{\infty} \frac{b\,(f_s)}{4} e^{j2\pi f_s t} df_s \tag{6}$$

where f_s denotes the signal frequencies. Here, A_{Rx} can be complex valued to account for complex modulation as well as chirped pulses arising from modulation or fiber dispersion. $t\ =\ 0$ is taken as the sampling time of the 1st symbol of the data sequence. The symbol specific formulas for the kth bit of the sequence are then given by

$$\mu\ f_N = \frac{\int_{f_s=-\infty}^{f_s=\infty} \int_{f_n=-\infty}^{f_n=\infty} \mathcal{F}_e(f_n)\left[\mathcal{F}_e\,(f_n) - \mathcal{F}_e\,(f_n - f_s)\right]^* \left|\mathcal{F}_o\,(f_n)\right|^2 df_n \frac{b}{2} e^{j2\pi f_s k\tau_{UI}}\, df_s}{2\left(A_{Rx} - \frac{a}{2}\right)} \tag{7}$$

where τ_{UI} is the unit interval and

$$\gamma\ f_N = \frac{\int_{f_{s1}=-\infty}^{f_{s1}=\infty} \int_{f_{s2}=-\infty}^{f_{s2}=\infty} Re\left(\int_{f_n=-\infty}^{f_n=\infty} \begin{bmatrix} \left|\mathcal{F}_e\,(f_n)\right|^2 \\ -\mathcal{F}_e\,(f_n - f_{s1})^*\, \mathcal{F}_e(f_n - f_{s2}) \end{bmatrix} \left|\mathcal{F}_o\,(f_n)\right|^2 df_n \frac{b(f_{s1})}{2} \frac{b(f_{s2})^*}{2} e^{j2\pi(f_{s1}-f_{s2})k\tau_{UI}}\right) df_{s1}\, df_{s2}}{4\left|A_{Rx} - \frac{a}{2}\right|^2} \tag{8}$$

The variance of the ASE-signal beat noise is then given by

$$\frac{\sigma^2}{4N_n} = \left|A_{Rx}\right|^2 f_F - \frac{a}{2} Re\left(\left(A_{Rx} - \frac{a}{2}\right)\mu\right) f_N - \frac{1}{2}\left|A_{Rx} - \frac{a}{2}\right|^2 \gamma f_N \tag{9}$$

In the evaluation of (7) and (8), care has to be taken to ensure that $t\ =\ 0$ corresponds to the sampling time *after* the electrical filter, not the optimum sampling time of the signal as described at the input of the Rx prior to detection (alternatively, one may define the electrical filter transfer function $\mathcal{F}_e$ such that it introduces no time delay, as explained earlier). The expressions of μf_N and γf_N can be seen to be simply weighted averages of the expressions of f_A and f_C, with the weights given by the Fourier coefficients of the complex valued signal field amplitude. In addition to the dependencies on baud rate, signal extinction ratio, optical cut-off frequency and electrical filter shape, that still hold here, a pattern dependency can be inferred from the above: Symbols embedded in a rapidly varying signal shape will have stronger noise mixing coefficients than symbols embedded in a constant signal. For example, in the case of NRZ OOK, the coefficients for an isolated '1' (in '..00100..') or an isolated '0' (in '..11011..') can be expected to be much higher than a '1' embedded in a string of ones (in '..11111..') or a '0' embedded in a string of zeros (in '..00000..'). In Section 4, it will be illustrated with numerical examples that categorizing NRZ OOK bits into three categories depending on whether they are (a) embedded in a string of three identical bits (zero nearby transitions), (b) have one immediately adjacent transition or (c) have two immediately adjacent transitions and deriving average coefficients for each category is typically sufficient to obtain high modeling accuracy.

Since the investigated modification of ASE-signal beat noise is particularly strong with electrical filters with a steep cut-off, it will be particularly pronounced when monitoring a signal with a real-time oscilloscope or when feeding the signal through other types of steep anti-aliasing filters, for example before an ADC in a DMT receiver. Thus, it is helpful to assess how the recorded signal quality factor will be modified by recording with an oscilloscope. For example, one may compare a linear, broadband electro-optical receiver followed by either an oscilloscope (resulting in a sizeable modification of the ASE-signal beat noise) or a wide bandwidth error detector from a bit error rate tester (BERT). In the latter case, the ASE-beat noise will be very close to the one derived from instantaneous signal levels if the error detector features a progressive roll-off or if it is sufficiently broadband so that its cutoff frequency approaches or exceeds the sum of the optical filter cutoff frequency f_{OF} with the maximum signal frequency $f_{\max}$ (if the cutoff frequency f_{EF} of the electrical

test system is larger than the sum of the optical cutoff frequency f_{OF} and the maximum signal frequency $f_{\max}$ prior to optical detection, the coefficients μ and γ are actually zero independently on the electrical filter steepness). This was for example identified as a source of discrepancies in Q-factor and BER measurements reported in [16].

Following procedure is assumed to be used to extract the signal Q-factor from the oscilloscope data: The recorded signal is first integrated over several identical data cycles in order to obtain a low noise version of the real-time signal. This low noise reference is then subtracted from the instantaneous signal traces in order to extract the instantaneous noise at the sampling times. Noise is further classified according to the symbol type and the noise std. dev. computed for each symbol category. The relevant modification of ASE-signal beat noise will then be given by (9) as averaged over all symbols of a given type.

To evaluate this, one possibility is to explicitly compute average coefficients based on (7) and (8). In Appendix III, equations for this average modified noise variance are however directly derived under the additional assumptions that (i) the data stream's optical field is composed of a linear superposition of otherwise independent symbols (no nonlinearities in the optical channel) and (ii) symbols are identically shaped modulo a symbol specific multiplicative factor. Equation (6) remains valid, with the additional condition

$$b\ (f_s) = \sum_k K_{S_k} \tilde{b}\,(f_s)\, e^{-i2\pi f_s k \tau_{UI}} \tag{10}$$

where the summation is taken over all the symbols of the sequence, K_{S_k} is the multiplicative factor associated to symbols of type S_k and $\tilde{b}(f_s)$ are the Fourier coefficients of an isolated symbol (this captures assumptions (i) and (ii) described above). We then get

$$\frac{\sigma_S^2}{4N_n} = \left\langle |A_{Rx}|^2 \right\rangle_S f_F - \frac{a}{2} Re\left(\left\langle A_{Rx} - a/2 \right\rangle_S \langle \mu \rangle\right) f_N - \frac{1}{2}\left|\left\langle A_{Rx} - a/2 \right\rangle_S\right|^2 \gamma_0 f_N$$
$$- \frac{1}{2M} \sum\nolimits_{S'} \left|\left\langle A_{Rx} - a/2 \right\rangle_{S'}\right|^2 (\langle \gamma \rangle - \gamma_0)\, f_N \tag{11}$$

where σ_S^2 is the average ASE-signal beat noise variance for symbols of type S, $\langle . \rangle_S$ are averages taken over all symbols of type S, M is the number of different symbol types and the summation is taken over all symbols, $\langle \mu \rangle$ is the effective average of μ and $\langle \gamma \rangle$ is the effective average of $\gamma \cdot \gamma_0$ is the value of γ taken for isolated symbols. Explicit formulas of these coefficients are given by

$$\langle \mu \rangle\ f_N = \frac{\int_{f_s=-\infty}^{f_s=\infty} \int_{f_n=-\infty}^{f_n=\infty} \mathcal{F}_e(f_n) \left[\mathcal{F}_e\,(f_n) - \mathcal{F}_e\,(f_n - f_s)\right]^* |\mathcal{F}_o\,(f_n)|^2 df_n \frac{\tilde{b}}{2} df_s}{\int_{f_s=-\infty}^{f_s=\infty} \frac{\tilde{b}}{2} df_s} \tag{12}$$

$$\langle \gamma \rangle\ f_N = \frac{\frac{1}{\tau_{UI}} \sum_{m=-\infty}^{\infty} \int_{f_{s1}=-\infty}^{f_{s1}=\infty} Re\left(\int_{f_n=-\infty}^{f_n=\infty} \left[|\mathcal{F}_e\,(f_n)|^2 - \mathcal{F}_e\,(f_n - f_{s1})^*\, \mathcal{F}_e\!\left(f_n - f_{s1} + \frac{m}{\tau_{UI}}\right)\right] |\mathcal{F}_o\,(f_n)|^2 df_n \frac{\tilde{b}(f_{s1})}{2} \frac{\tilde{b}\left(f_{s1} - \frac{m}{\tau_{UI}}\right)^*}{2} \right) df_{s1}}{\left| \int_{f_s=-\infty}^{f_s=\infty} \frac{\tilde{b}}{2} df_s \right|^2} \tag{13}$$

$$\gamma_0\ f_N = \frac{\int_{f_{s1}=-\infty}^{f_{s1}=\infty} \int_{f_{s2}=-\infty}^{f_{s2}=\infty} Re\left(\int_{f_n=-\infty}^{f_n=\infty} \left[|\mathcal{F}_e\,(f_n)|^2 - \mathcal{F}_e\,(f_n - f_{s1})^*\, \mathcal{F}_e(f_n - f_{s2})\right] |\mathcal{F}_o\,(f_n)|^2 df_n \frac{\tilde{b}(f_{s1})}{2} \frac{\tilde{b}(f_{s2})^*}{2} \right) df_{s1} df_{s2}}{\left| \int_{f_s=-\infty}^{f_s=\infty} \frac{\tilde{b}}{2} df_s \right|^2} \tag{14}$$

These formulas are directly applicable to multi-level NRZ signaling and are compatible with the modeling of fiber dispersion and other forms of linear inter-symbol interference (ISI). They are however incompatible with the rigorous modeling of optical channel nonlinearities as arising for example in a saturating SOA.

Since the modification of the ASE-signal beat noise is particularly pronounced for electrical filters with steep transfer functions, simplified formulas for the extreme case of a square shaped transfer

function are given below. These are directly applicable to the case of monitoring of an optical signal with a wideband linear receiver followed by a lower bandwidth real time oscilloscope or lower bandwidth anti-aliasing filter. Assuming both the optical and the electrical filters to have square transfer functions, the optical filter to have a passband $2f_{OF}$ and a single sided cutoff frequency f_{OF}, i.e., further assuming the optical carrier to be centered relative to the optical filter transfer function, and assuming the electrical filter to have a cutoff frequency f_{EF}, (7) converts into

$$\mu\, f_N = \frac{\int_{f_s=-\infty}^{f_s=\infty} \min\left(|f_s|, 2f_{EF}\right) \frac{b}{2} df_s}{2\left(A_{Rx} - \frac{a}{2}\right)} \tag{15}$$

for $f_{OF} \geq f_{EF}$ and

$$\mu\, f_N = \frac{\int_{f_s=-\infty}^{f_s=\infty} \min\left(\max\left(0, |f_s| - (f_{EF} - f_{OF})\right), 2f_{OF}\right) \frac{b}{2} df_s}{2\left(A_{Rx} - \frac{a}{2}\right)} \tag{16}$$

for $f_{OF} < f_{EF}$. Note that it would seem natural to restrict the integration domain in (16) to $[-f_{OF}, f_{OF}]$ since the signal is also filtered by the optical filter, however, as mentioned earlier, the optical filter shape in the general case can be chosen to sculpt the targeted ASE spectrum, while the signal spectrum is independently described at the input of the Rx prior to photodetection, leaving maximum flexibility in the described process. In the case where both $f_{OF} \geq f_{EF}$ and $2f_{EF}$ is larger than the maximum signal frequency, μf_N can be seen to simply reduce to a weighted average of the signal frequencies f_s weighted by the signal Fourier coefficients. Simplified formulas are given for γ and $\langle\gamma\rangle$ in Appendix II for the special cases $f_{OF} = \infty$ and $f_{OF} = f_{EF}$. For an arbitrary f_{OF}, but assuming $f_{\max} \leq f_{EF}$, we obtain

$$\gamma\, f_N = 2Re(\mu)\, f_N - \frac{\frac{1}{4}\int_{f_{s1}=0}^{f_{s1}=\infty}\int_{f_{s2}=0}^{f_{s2}=\infty} \left(\min\left(f_{s1}, f_{s2}\right) + \min\left(f_{s1}, f_{s2}, f_{OF} - f_{EF}\right)\right) Re\left(b\left(f_{s1}\right) b(f_{s2})^* + b\left(-f_{s1}\right) b(-f_{s2})^*\right) df_{s1}\, df_{s2}}{4|A_{Rx} - a/2|^2} \tag{17}$$

if $f_{OF} \geq f_{EF}$ and

$$\gamma\, f_N = 2Re(\mu)\, f_N - \frac{\frac{1}{4}\int_{f_{s1}=0}^{f_{s1}=\infty}\int_{f_{s2}=0}^{f_{s2}=\infty} \left(\max\left(\min\left(f_{s1} - f_{EF} + f_{OF}, f_{s2} - f_{EF} + f_{OF}\right), 0\right)\right) Re\left(b\left(f_{s1}\right) b(f_{s2})^* + b\left(-f_{s1}\right) b(-f_{s2})^*\right) df_{s1}\, df_{s2}}{4|A_{Rx} - a/2|^2} \tag{18}$$

if $f_{OF} < f_{EF}$.

Here too, the second term in (17) (the equivalent of f_B) reduces to a simple weighted average of $\min(f_{s1}, f_{s2})$ weighted by $Re(b(f_{s1})\, b(f_{s2})^*)$ for large f_{OF}, so that both (15) and (17) can be seen to be simple extensions of (5) in that case. The same holds for arbitrary values of f_{OF} and f_{EF}: μf_N and $2Re(\mu) f_N - \gamma f_N$ are weighted averages of f_A and f_B, respectively weighted by b and by $Re(b(f_{s1})\, b(f_{s2})^*)$.

Fig. 2 shows numerical values for $\langle\mu\rangle$ and $\langle\gamma\rangle$ assuming an OOK NRZ data stream with initially perfectly square shaped symbols optically pre-filtered with a perfectly square shaped filter with single sided cutoff frequency $f_{\max}$ (i.e., the symbols have a sinc shaped Fourier transform truncated at frequencies above $f_{\max}$) prior to being optically amplified (i.e., this optical filter is part of the Tx model and is different from the post-amplification optical filter with passband $2f_{OF}$). In this case $|\langle A_{Rx} - a/2\rangle_0|^2 = |\langle A_{Rx} - a/2\rangle_1|^2$ and $-\frac{1}{2}|\langle A_{Rx} - a/2\rangle_S|^2 \gamma_0 f_N - \frac{1}{2M}\sum_{S'} |\langle A_{Rx} - a/2\rangle_{S'}|^2 (\langle\gamma\rangle - \gamma_0) f_N$ simplifies into $-\frac{1}{2}|\langle A_{Rx} - a/2\rangle_S|^2 \langle\gamma\rangle f_N$, i.e., μ and γ can be simply replaced by $\langle\mu\rangle$ and $\langle\gamma\rangle$ in (9), resulting in

$$\frac{\sigma_{0/1}^2}{4N_n} = \langle|A_{Rx}|^2\rangle_{0/1}\, f_F - \frac{a}{2} Re\left(\langle A_{Rx} - a/2\rangle_{0/1} \langle\mu\rangle\right) f_N - \frac{1}{2}\left|\langle A_{Rx} - a/2\rangle_{0/1}\right|^2 \langle\gamma\rangle f_N \tag{19}$$

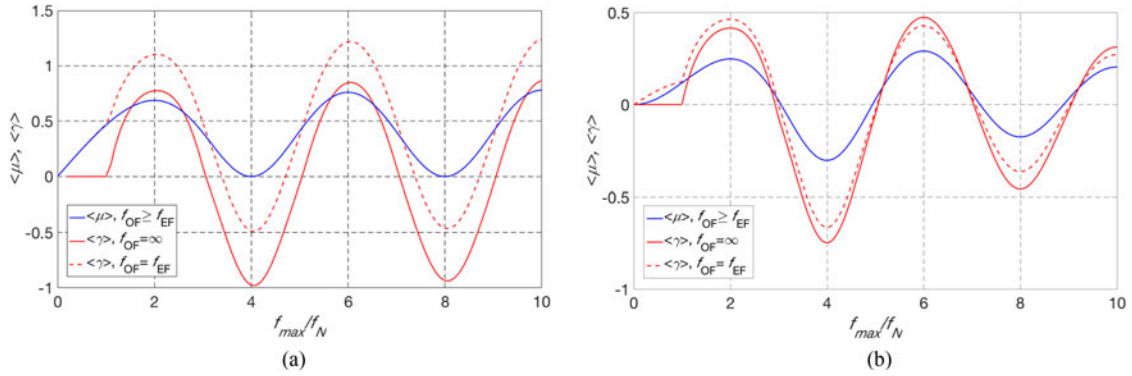

Fig. 2. Numerical evaluation of the noise mixing parameters $\langle\mu\rangle$ and $\langle\gamma\rangle$ as a function of $f_{\max}/f_N$ assuming the signal PSD to correspond to initially square shaped NRZ OOK symbols pre-filtered by an ideal square shaped optical filter with cutoff frequency $f_{\max}$. (a) Both electrical and optical filters are assumed to have a square transfer function. The electrical filter is assumed to satisfy the condition $f_{EF} \geq f_{\max}/2$ for $\langle\mu\rangle$ and the more restrictive condition $f_{EF} \geq f_{\max}$ for $\langle\gamma\rangle$. Two cases of optical filtering are considered for $\langle\gamma\rangle$, an infinite optical filter bandwidth (continuous red curve) and an optical filter with an ideal square shaped transfer function and $f_{OF} = f_{EF}$ (dashed red curve). Both assumptions result in the same value for $\langle\mu\rangle$ that remains unchanged in the whole range $f_{OF} \geq f_{EF}$. (b) The electrical filter is replaced by a 3rd order Butterworth filter with a cutoff frequency $2f_N$. For the dashed curve corresponding to $f_{OF} = f_{EF}$, the optical filter transfer function is also assumed to be a third order Butterworth.

This simple numerical example illustrates the order of magnitude of the coefficients as well as their dependency on the signal spectrum. In (a), both the electrical and optical filter are assumed to be ideal square shaped filters. Assuming $f_{OF} = f_{EF} = 2\,f_N = f_{\max}$, we obtain for example $\langle\mu\rangle = 0.6881$ and $\langle\gamma\rangle = 1.104$ (0.7756 without optical filter). Assuming a signal with infinite extinction ratio, this results in a penalty of 0.42 dBQ (1.0 dBQ without optical filter). (b) shows the coefficients after the electrical filter has been replaced by a third order Butterworth filter with the same cutoff frequency $2f_N$. At $f_{\max} = 2f_N$, the coefficients drop significantly to $\langle\mu\rangle = 0.2482$ and $\langle\gamma\rangle = 0.4633$ (0.4156 without optical filter) due to the reduced electrical filter steepness. Assuming again a signal with infinite extinction ratio, the penalty drops to 0.13 dBQ (0.36 dBQ without optical filter).

3. Experimental Validation

In order to verify the models described in the previous section, we performed an experiment consisting in modulating an optical carrier with a commercial Mach-Zehnder Modulator (Gigoptix LX8401 with an analog cut-off frequency of 33.5 GHz). After optical filtering with a 40 GHz passband filter ($f_{OF} =$ 20 GHz in the convention of the previous section), the signal was transduced by a high-speed U2T/Finisar XPRV2021A 40 GHz photoreceiver and imaged with a 21 GHz bandwidth real time oscilloscope. PRBS-7 pseudo-random bit sequences with data rates between 4 and 32 Gbps were applied to the modulator. By subtracting a time averaged PRBS-7 sequence from the real-time traces, 0- and 1-level noise statistics could be extracted from the eye diagrams (effectively corresponding to an average of noise variances over differing patterns). The modulator was biased to obtain an extinction ratio of 15 dB.

Fig. 3(a) shows the results: It can be seen that, as predicted, the 0-level noise std. dev. grows with the data rate, while the 1-level noise std. dev. is reduced. The sum $\sigma_0 + \sigma_1$ also grows, as expected. The continuous lines show a fit based on (19) with $\langle\mu\rangle = 0.58$ and $\langle\gamma\rangle = 0.5$ as numerically evaluated based on the assumption of a square oscilloscope transfer function, the measured optical filter transfer function, as well as the recorded signal shape. The deviation of the 0-level noise std. dev. for data rates above 25 Gbps is attributed to a reduction of the signal extinction ratio due to partial clipping of the signal by the 40 GHz optical filter (this can also be modeled by (19) by modifying

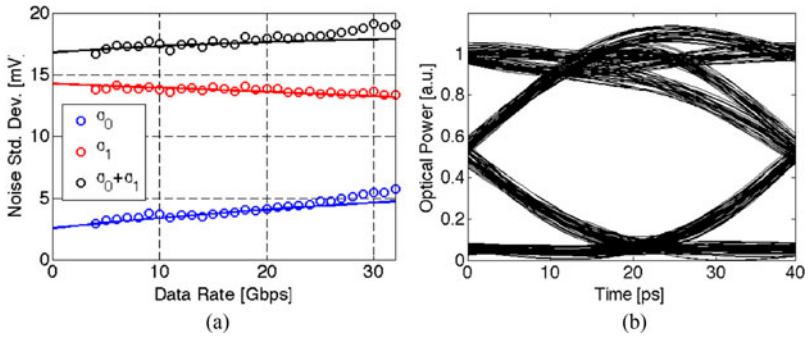

Fig. 3. (a) 0- and 1-level noise std. dev. as extracted from eye diagrams recorded with a real-time oscilloscope at different data rates (circles). Continuous lines show fits based on (19). (b) Eye diagram from the experimental Tx-out signal trace utilized for the numerical modeling in Section 4.

$A_{Rx,0}$ as a function of data rate to take the reduced extinction ratio at the input port of the Rx into account). The signal penalty at 25 Gbps, as compared to the Q-factor at low data rates below 4 Gbps, is 0.5 dBQ.

4. Numerical Examples

In order to further investigate the magnitude of the effect for different filter and signal shapes, we numerically modeled the effect of electrical and optical filtering on the signal-ASE beat noise of the signal with eye diagram shown in Fig. 3(b). This signal trace was experimentally recorded with the same setup as described above, with the only difference that the Mach-Zehnder modulator was replaced by a resonant ring modulator (RRM). The distortion seen in the eye diagram at the 1-level is due to the peaking in the electro-optic S_{21} of the RRM [24], [25]. From the data pattern dependent noise levels, the data pattern dependent coefficients μ and γ can be extracted based on

$$\mu = -2\frac{\left(\sigma_1^2 - \sigma_0^2\right) - \left(\bar{\sigma}_1^2 - \bar{\sigma}_0^2\right)}{\left(\bar{\sigma}_1^2 - \bar{\sigma}_0^2\right)}\frac{f_F}{f_N} \tag{20}$$

$$\gamma = -4\frac{\left(\sigma_1^2 + \sigma_0^2\right) - \left(\bar{\sigma}_1^2 + \bar{\sigma}_0^2\right)}{\left(\overline{\sigma_1} - \overline{\sigma_0}\right)^2}\frac{f_F}{f_N} \tag{21}$$

In these formulas, σ_0 and σ_1 respectively correspond to the 0-level and 1-level signal-ASE beat noise recorded from '0' and '1' bits of exactly inverted data streams. E.g., if the 0-level noise is recorded from the third bit in the sequence '01001', the 1-level noise is recorded from the third bit of the sequence '10110'. This exact attribution is required in order to discuss pattern dependent effects in the following.

Figs. 4(a), (b) and (c) show the results assuming a 20 GHz square shaped electrical filter emulating the real-time oscilloscope, as well as the measured transfer function of the 40 GHz optical filter. Furthermore, a 15 dB extinction ratio is assumed as in the experiment described above, as well as a data rate of 25 Gbps. Histograms are shown for the extracted coefficients μ and γ, as well as for the Q-factor penalty in dBQ. Since the results depend strongly on whether the bits see 0, 1 or 2 transitions to their immediately adjacent neighbors, separate histograms are shown (black for 0 transitions, blue for 1 transition and red for 2 transitions). It should be noted that these classes apply to respectively 25%, 50% and 25% of the bits, so that they should not be considered as rare pattern specific occurrences.

As can be seen in Figs. 4(a) and (b), the coefficients μ and γ are close to zero for bits with no transitions to adjacent bits and take their largest values for bits with two transitions, as expected. Moreover, while the average coefficients are given by $\langle\mu\rangle \cong 0.58$ and $\langle\gamma\rangle \cong 0.5$, the coefficients for bits with two adjacent transitions are given by $\mu \cong 1$ and $\gamma \cong 1$. This ought not to be surprising, as rapidly changing bit sequences essentially correspond to the simplified signal first assumed in the

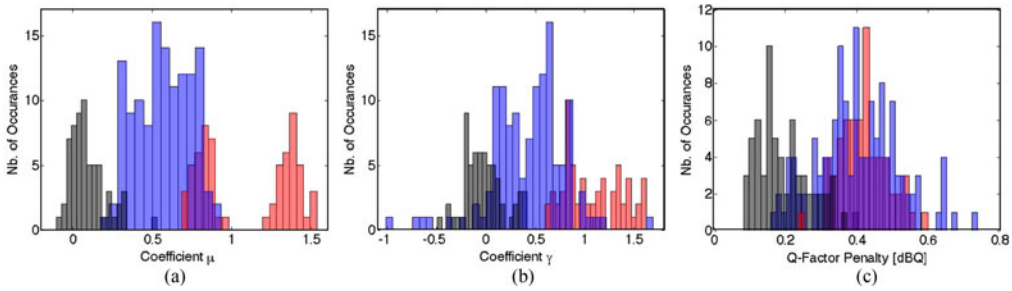

Fig. 4. Bit specific coefficients μ and γ and bit specific Q-factor penalty extracted from the numerical experiment described in the text. Bits with zero, one and two transitions to immediately adjacent bits are respectively shown in black, blue and red.

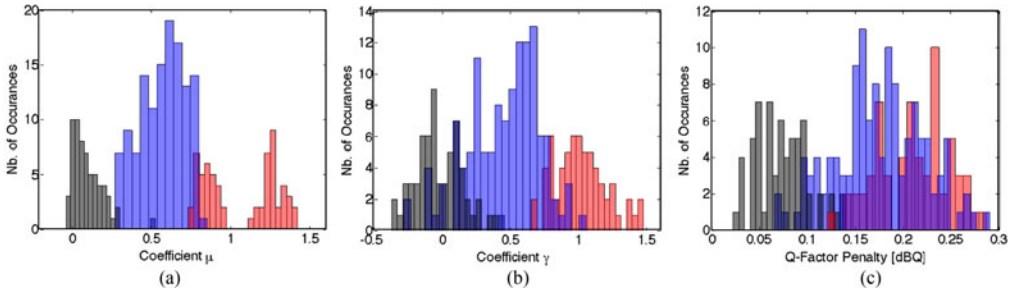

Fig. 5. Bit specific coefficients μ and γ and bit specific Q-factor penalty extracted from the numerical experiment described in the text. Bits with zero, one and two transitions to immediately adjacent bits are respectively shown in black, blue and red. The baseline configuration from Fig. 4 was modified by reducing the signal extinction ratio from 15 to 9 dB.

derivation of (4), that can be approximated by (5) here. Importantly, since these bit sequences also typically feature the worst-case increase of $\sigma_0 + \sigma_1$, the simplified (4) can also be taken to yield a first estimate on the Q-factor quality reduction. It might be puzzling why μ features two disjoint distributions in the case of bits with two adjacent transitions: These correspond to 0-bits in '101' and 1-bits in '010', that behave differently here due to the different signal shapes (primarily due to the peaking in the RRM transfer function when operated in the large signal regime, that only occurs at the optical 1-levels). As expected, the bits with the higher coefficients also have the higher noise penalties, as seen with the blue and red distributions in Fig. 4(c). The difference between bits with 1 or 2 transitions is less pronounced here, as a larger μ results in a higher penalty, but a larger γ results in a lower penalty, i.e., the two trends partially offset each other. The calculated penalty, on the order $\sim$0.4 dBQ for bits with 1 and 2 transitions (i.e., for ¾ of the bits), is in line with the measurements reported above ($\sim$0.5 dBQ).

We can now introduce a couple of changes relative to this baseline scenario to exemplify the impact of different parameters in a realistic situation:

Two other characteristics of the setup, the signal extinction ratio and the electrical filter edge steepness, have a drastic effect on the Q-factor penalty: In Fig. 5, the signal extinction ratio was reduced to 9 dB, but the signal and filter shapes left otherwise unchanged compared to the baseline case: A constant was added to the optical field amplitude rather than to the optical power, to leave the coefficients μ and γ, as predicted by the analytical formulas, unchanged. Indeed, this is confirmed to be the case (compare Figs. 5(a) and (b) with 4(a) and (b)). There is some scatter in the histograms due to the stochastic nature of the evaluation, the average coefficient values remain however unchanged at $\langle\mu\rangle = 0.58$ and $\langle\gamma\rangle = 0.5$. The Q-factor penalty is however drastically reduced as a consequence of (9).

As a final test, we changed the square shaped electrical filter in the baseline configuration by replacing it with a 3rd order Butterworth filter with the same 3 dB cutoff frequency (Fig. 6). The

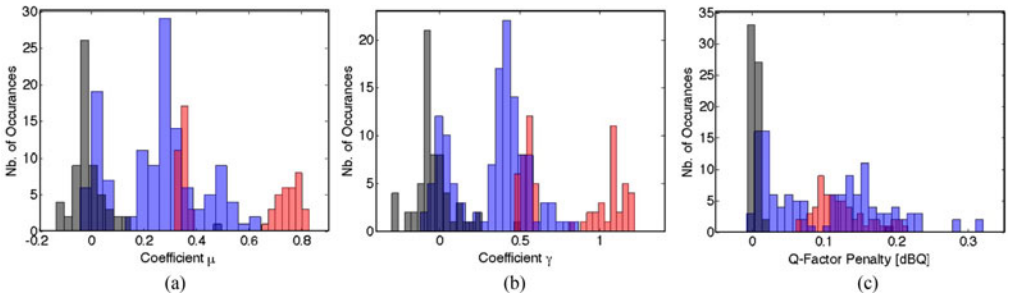

Fig. 6. Bit specific coefficients μ and γ and bit specific Q-factor penalty extracted from the numerical experiment described in the text. Bits with zero, one and two transitions to immediately adjacent bits are respectively shown in black, blue and red. The baseline configuration from Fig. 4 was modified by replacing the square shaped electrical filter by a third order Butterworth filter.

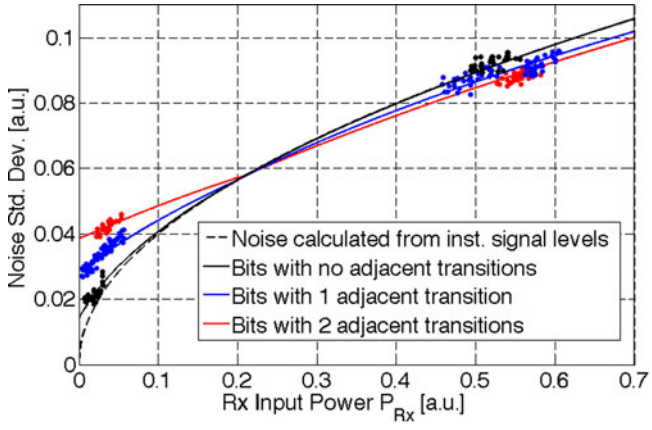

Fig. 7. Numerically simulated and modeled ASE-signal beat noise levels. Simulated data is from the same numerical experiment as shown in Fig. 4.

other settings were left unchanged relative to the baseline case (i.e., 15 dB extinction ratio). The average coefficients are drastically reduced to $\langle\mu\rangle = 0.26$ and $\langle\gamma\rangle = 0.37$. μ in particular is strongly reduced, both for bits with one and two adjacent bit transitions. As a consequence, even though the extinction ratio remains 15 dB, the penalty associated to the modification of ASE-signal noise becomes quite small.

Given the pattern dependence of the coefficients μ and γ (i.e., the dependence on nearby transitions), one may wonder whether (9) can be used to obtain accurate results without having to recalculate μ and γ for every single pattern. In fact, once bits have been categorized into bits with zero, one or two adjacent transitions, and coefficients μ and γ have been determined for each category, the remaining discrepancy between predictions and the ASE-signal beat noise recorded from numerical simulations is reasonably small (see Fig. 7). As an additional refinement, bits have also been categorized into '0' and '1' bits. This additional categorization takes into account the asymmetry of the signal shapes (which is also reflected in (11) when $|\langle A_{Rx} - a/2\rangle_{'0'}|^2 \neq |\langle A_{Rx} - a/2\rangle_{'1'}|^2$ by the inclusion of coefficient γ_0).

In the evaluation of (9), average values of the coefficients μ and γ were taken depending on the number of immediately adjacent bit transitions and on the polarity of the bits (i.e., one of six possibilities for each coefficient), however A_{Rx} was taken as the actual instantaneous value of the signal. This can be seen to improve the modeling predictions, as the recorded noise from the "numerical experiment" not only forms a point cloud lying on the modeling curves, but actually tracks the prediction curves as a function of the signal power $P_{Rx} = |A_{Rx}|^2$. Variations of A_{Rx} for a given bit polarity are due to ISI as caused by bandwidth limitations associated to the driving and operation

of the RRMs as well as by clipping of the signal spectrum by the optical ASE reduction filter in the experimental setup in which the assumed signal shape was recorded.

As can be seen, the predictions resulting from these six sets of parameters coincide with the numerically modeled ASE-signal beat noise levels quite well (four sets of parameters need to be determined in practice since the average coefficients for the bits without adjacent transitions can be assumed to be zero without much loss in accuracy).

5. Full Link Model With ASE-ASE Noise and Comparison of Modeling With and Without Gaussian Approximation

In order to verify the practical relevance of the corrections investigated here, we made the following "numerical experiments" to compare the magnitude of the error due to the Gaussian noise approximation to the magnitude of the correction associated to modification of the level dependent ASE-signal beat noise due to electrical filtering. The modeled link corresponds to the following: An initial square shaped OOK NRZ signal is first electrically filtered (truncation of Fourier spectrum at frequencies above $2f_N$ followed by filtering with a single pole filter with a cutoff frequency f_N) prior to being transduced by a Mach-Zehnder modulator operated at its quadrature point, assuming the electrical drive signal to be sufficiently strong to reach full extinction. After amplification, it is filtered by a square shaped optical filter with $f_{OF} = 2f_N$, transduced with an ideal photodetector and filtered by a square shaped electrical filter, also with $f_{EF} = 2f_N$. The BER is estimated in four different ways as a function of decision threshold: (i) semi-analytically with the Gaussian approximation, with the variance of the total noise estimated by summing the variance of the ASE-ASE beat noise with the variance of the unmodified ASE-signal beat noise, i.e., as calculated from the instantaneous signal levels with (2); (ii) semi-analytically with the Gaussian approximation, with the variance of the total noise estimated by summing the variance of the ASE-ASE beat noise with the variance of the modified ASE-signal beat noise, i.e., as calculated from (9); (iii) numerically, calculating the ASE-ASE beat noise and summing it to the unmodified ASE-signal beat noise, taking the non-Gaussian distribution of ASE-ASE beat noise and its correlation with ASE-signal beat noise into account, followed by numerical error counting; and (iv) numerically, calculating the ASE-ASE beat noise and summing it to the modified ASE-signal beat noise, taking the non-Gaussian distribution of ASE-ASE beat noise and its correlation with ASE-signal beat noise into account, followed by numerical error counting. The ASE noise level was dialed in so as to obtain a BER in the 10^{-3} to 10^{-4} range.

Results are shown in Fig. 8. It can be seen that, as expected, the Gaussian noise approximation introduces a large error in the estimation of the optimum threshold, but has little effect on the BER. Taking the modification of the ASE-signal beat noise into account further shifts the optimum threshold towards higher values. The effect on the estimated BER is however much more pronounced (5X) and close to the value obtained by error counting (same small error due to the Gaussian approximation). The modification of the ASE-signal beat noise by itself accounts for almost half an order of magnitude increase in the BER. Cumulative effects with other small measurement biases, such as a modest inter-symbol interference increase due to filtering in the instrument and a resulting reduction in vertical eye height, could easily lead to an order of magnitude error in the estimated BER [16].

6. Conclusion

In conclusion, we have derived a set of compact equations describing the effect of optical and electrical filtering on level dependent ASE-signal beat noise in direct detection systems. Importantly, this effect results in a further reduction of signal quality that should be taken into account for accurate system modeling, particularly when electrical filters with a steep transfer function, such as anti-aliasing filters in a real-time oscilloscope or before analog-to-digital conversion, are utilized. General trends in the predictions were verified by experiment with an NRZ OOK data stream.

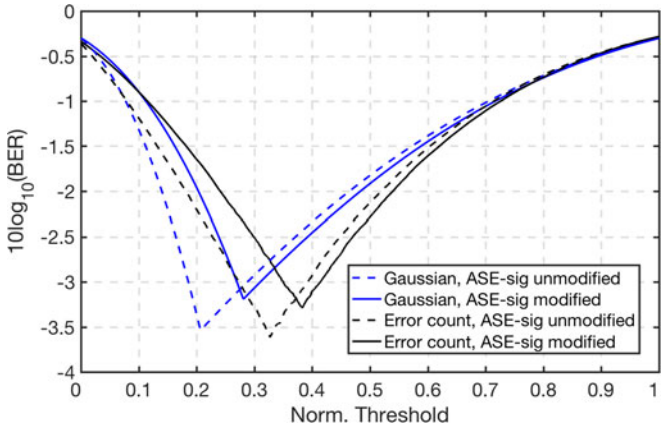

Fig. 8. BER as a function of decision threshold for four models, either taking the modification of the signal-ASE beat noise into account (solid lines) or using the unmodified signal-ASE beat noise derived from instantaneous signal levels (dashed lines), as well as based on the Gaussian noise approximation (blue curves) or on a complete noise model taking the chi square distribution of ASE-ASE beat noise and its correlation to ASE-signal noise into account (black curves, evaluated with numerical error counting).

Numerical signal flow modeling was used to exemplify the magnitude of the noise level modification in different system configurations and to explore pattern dependencies. General formulas reported in this paper are applicable to arbitrary complex valued data streams and compatible with the modeling of multi-level signaling.

Acknowledgment

The authors would like thank the European Commission for funding the project “Broadband Integrated and Green Photonic Interconnects for High-Performance Computing and Enterprise Systems” (BIG PIPES) under the seventh framework with contract no. 619591.

References

[1] D. Marcuse, “Derivation of analytical expressions for the bit-error probability in lightwave systems with optical amplifiers,” *J. Lightw. Technol.*, vol. 8, no. 12, pp. 1816–1823, Dec. 1990.
[2] P. A. Humblet and M. Azizoglu, “On the bit error rate of lightwave systems with optical amplifiers,” *J. Lightw. Technol.*, vol. 9, no. 11, pp. 1576–1582, Nov. 1991.
[3] N. S. Bergano, F. W. Kerfoot, and C. R. Davidson, “Margin measurements in optical amplifier systems,” *Photon. Technol. Lett.*, vol. 5, no. 3, pp. 304–306, 1993.
[4] S. Saito, T. Matsuda, and A. Naka, “An analytical signal and noise expression for optical preamplifier receivers and its application,” in *Proc. Opt. Amplifiers Appl.*, 1997, Paper TuD11.
[5] L. Boivin and G. J. Pendock, “Receiver sensitivity for optically amplified RZ signals with arbitrary duty cycle,” in *Proc. Opt. Amplifiers Appl.*, 1999, Paper ThB4.
[6] P. J. Winzer, M. Pfennigbauer, M. M. Strasser, and W. R. Leeb, “Optimum filter bandwidths for optically preamplified NRZ receivers,” *J. Lightw. Technol.*, vol. 19, no. 9, pp. 1263–1273, Sep. 2001.
[7] J. L. Rebola and A. V. T. Cartaxo, “Gaussian approach for performance evaluation of optically preamplified receivers with arbitrary optical and electrical filters,” in *IEEE Proc. Optoelectron.*, vol. 148, no. 3, pp. 135–142, Jun. 2001.
[8] M. Pfennigbauer, M. M. Strasser, M. Pauer, and P. J. Winzer, “Dependence of optically preamplified receiver sensitivity on optical and electrical filter bandwidths – measurement and simulations,” *IEEE Photon. Technol. Lett.*, vol. 14, no. 6, pp. 831–833, Jun. 2002.
[9] J.-S. Lee and C.-S. Shim, “Bit-error-rate analysis of optically preamplified receivers using an eigenfunction expansion method in optical frequency domain,” *J. Lightw. Technol.*, vol. 12, no. 7, pp. 1224–1229, Jul. 1994.
[10] L. F. B. Ribeiro, J. R. F. Rocha, and J. L. Pinto, “Performance evaluation of EDFA preamplified receivers taking into account intersymbol interference,” *J. Lightw. Technol.*, vol. 13, no. 2, pp. 225–232, Feb. 1995.
[11] S. L. Danielsen, B. Mikkelsen, T. Durhuus, C. Joergensen, and K. E. Stubkjaer, “Detailed noise statistics for an optically preamplified direct detection receiver,” *J. Lightw. Technol.*, vol. 13, no. 5, pp. 977–981, May 1995.
[12] I. T. Monroy and G. Einarsson, “Bit error evaluation of optically preamplified direct detection receivers with fabry-perot optical filters,” *J. Lightw. Technol.*, vol. 15, no. 8, pp. 1546–1553, Aug. 1997.
[13] E. Forestieri, “Evaluating the error probability in lightwave systems with chromatic dispersion, arbitrary pulse shape and pre- and postdetection filtering,” *J. Lightw. Technol.*, vol. 18, no. 11, pp. 1493–1503, Nov. 2000.

[14] F. Abramovich and P. Bayvel, "Some statistical remarks on the derivation of BER in amplified optical communication systems," *IEEE Trans. Commun.*, vol. 45, no. 9, pp. 1032–1034, Sep. 1997.
[15] P. Angelini *et al.*, "64-Gb/s optical transmission using DFB-EAM transmitter and SOA-PIN-TIA receiver with -23.5-dBm record sensitivity," in *Proc. 2106 Eur. Conf. Opt. Commun.*, Sep. 2016, pp. 205–207.
[16] A. Moscoso-Mártir *et al.*, "Silicon photonics transmitter with SOA and semiconductor mode-locked laser," *Sci. Rep.*, vol. 7, Oct. 2017, Art. no. 13857.
[17] A. Moscoso-Mártir, J. Müller, E. Islamova, F. Merget, and J. Witzens, "Calibrated link budget of a silicon photonics WDM transceiver with SOA and semiconductor mode-locked laser," *Sci. Rep.*, vol. 7, Sep. 2017, Art. no. 12004.
[18] J.-H. Han, F. Boeuf, J. Fujikata, S. Takahashi, S. Takagi, and M. Takenaka, "Efficient low-loss InGaAsP/Si hybrid MOS optical modulator," *Nature Photon.*, vol. 11, pp. 486–490, Jul. 2017.
[19] T. Hiraki *et al.*, "Heterogeneously integrated III–V/Si MOS capacitor mach-zehnder modulator," *Nature Photon.*, vol. 11, pp. 482–485, Jul. 2017.
[20] J. Witzens, "Silicon photonics: Modulators make efficiency leap," *Nature Photon.*, vol. 11, pp. 459–462, Jul. 2017.
[21] R. Ding *et al.*, "Demonstration of a low VπL modulator with GHz bandwidth based on electro-optic polymer-clad silicon slot waveguides," *Opt. Exp.*, vol. 18, no. 15, pp. 15618–15623, Jul. 2010.
[22] R. Palmer *et al.*, "High-speed, low drive-voltage silicon-organic hybrid modulator based on a binary-chromophore electro-optic material," *J. Lightw. Technol.*, vol. 32, no. 16, pp. 2726–2734, Aug. 2014.
[23] M. N. Ngo *et al.*, "Electro absorption modulated laser integrated with a semiconductor optical amplifier for 100-k 10.3 Gb/s dispersion-penalty-free transmission," *J. Lightw. Technol.*, vol. 31, no. 2, pp. 232–238, Jan. 2013.
[24] Q. Xu, S. Manipatruni, B. Schmidt, J. Shakya, and M. Lipson, "12.5 Gbit/s carrier-injection-based silicon micro-ring silicon modulators," *Opt. Exp.*, vol. 15, no. 2, pp. 430–436, Jan. 2007.
[25] J. Müller *et al.*, "Optical peaking enhancement in high-speed ring modulators," *Sci. Rep.*, vol. 4, Sep. 2014, Art. no. 06310.